RESEARCH ARTICLE | MARCH 26 2025

Pressure effects on the electronic structure of the kagome metal CsV_3Sb_5

Shalika R. Bhandari ; Vivek Gusain ; Mohd Zeeshan; D. P. Rai ; Keshav Shrestha

APL Quantum 2, 016133 (2025)
https://doi.org/10.1063/5.0255919

Pressure effects on the electronic structure of the kagome metal CsV_3Sb_5

Cite as: APL Quantum 2, 016133 (2025); doi: 10.1063/5.0255919
Submitted: 31 December 2024 • Accepted: 9 March 2025 •
Published Online: 26 March 2025

View Online Export Citation CrossMark

Shalika R. Bhandari,[1] Vivek Gusain,[2] Mohd Zeeshan,[2] D. P. Rai,[3] and Keshav Shrestha[4,a)]

AFFILIATIONS

[1] Department of Physics, Bhairahawa Multiple Campus, Tribhuvan University, Siddarthanagar, 32900 Rupandehi, Nepal
[2] Department of Physics, Indian Institute of Technology, Hauz Khas, New Delhi 110016, India
[3] Department of Physics, Mizoram University, Aizawl 796004, India
[4] Department of Chemistry and Physics, West Texas A&M University, Canyon, Texas 79016, USA

[a)] Author to whom correspondence should be addressed: kshrestha@wtamu.edu

ABSTRACT

This study explores the electronic and structural properties of the kagome metal CsV_3Sb_5 under uniaxial pressures up to 20 GPa, utilizing first-principles calculations based on experimental crystallographic data provided by Tsirlin *et al.*, SciPost Phys. **12**, 049 (2022). At ambient pressure, the electronic band structure exhibits multiple Dirac points, van Hove singularities (VHSs), and flat bands near the Fermi level, which progressively shift closer to the Fermi level with increasing pressure. Remarkably, two additional Dirac-like crossings emerge above 4.9 GPa, moving ~25 meV below the Fermi level at 20 GPa. Concurrently, the VHS crosses the Fermi level as pressure increases to 9.8 GPa, highlighting a dynamic evolution of the electronic structure under high pressure conditions. The Fermi surface evolution under pressure reveals quasi-2D pockets, including a deformed cylindrical pocket centered at the Γ-point and a hexagonal pocket at the Brillouin zone boundary. Notably, the cylindrical pocket splits into two semi-spherical pockets above 4.9 GPa. Phonon calculations indicate lattice dynamical instability at ambient pressure, as evidenced by negative phonon frequencies, but stabilization occurs above 4.9 GPa, where all phonon modes become positive. These findings provide crucial insights into the pressure-induced modifications in the electronic and structural properties of CsV_3Sb_5, advancing the understanding of kagome-based quantum materials and their emergent phenomena.

I. INTRODUCTION

In recent years, kagome metals have attracted significant research interest in condensed matter physics and materials engineering due to their unique electronic properties, which are characterized by a frustrated lattice geometry.[1–3] Materials with kagome lattices are known to host multiple exotic quantum states, such as non-trivial topology, charge-density wave (CDW) order, unconventional superconductivity, and more.[2,4] In particular, 1:3:5-type layered kagome metals, also known as the 135 family, with the chemical formula AV_3Sb_5 (A = K, Rb, and Cs), exhibit CDW order, superconductivity, an anomalous Hall effect, flat bands, and van Hove singularities (VHSs)[5–8] near the Fermi level. Within the AV_3Sb_5 series, CsV_3Sb_5 demonstrates CDW and superconductivity below 94 and 2.5 K,[8,9] respectively. A distinctive feature of these compounds is the proximity of the Fermi level to Dirac points and VHSs, as revealed by several recent density functional theory (DFT) studies.[10–13] The intricate coupling between CDW order and superconductivity in AV_3Sb_5 has sparked extensive research to understand the mechanisms driving these transitions.[2,3]

CsV_3Sb_5 is a representative kagome metal that crystallizes in a layered structure comprising a mixture of triangular and hexagonal networks, forming an intermetallic kagome compound, as illustrated in Fig. 1(a). In the two-dimensional (2D) kagome network of V atoms, Sb is intercalated within the triangular lattices, while Cs atoms occupy the corners of the unit cell, creating a hexagonal-prismatic layered symmetry with the space group $P6/mmm$ (191). There are two types of Sb atoms: Sb1, located in the plane of the V-atoms, and Sb2, positioned out of the plane. The vanadium kagome network is interwoven with a simple hexagonal network formed by Sb1 sites. From a space-filling perspective, the Sb1 atoms occupy the natural gaps within the kagome plane.

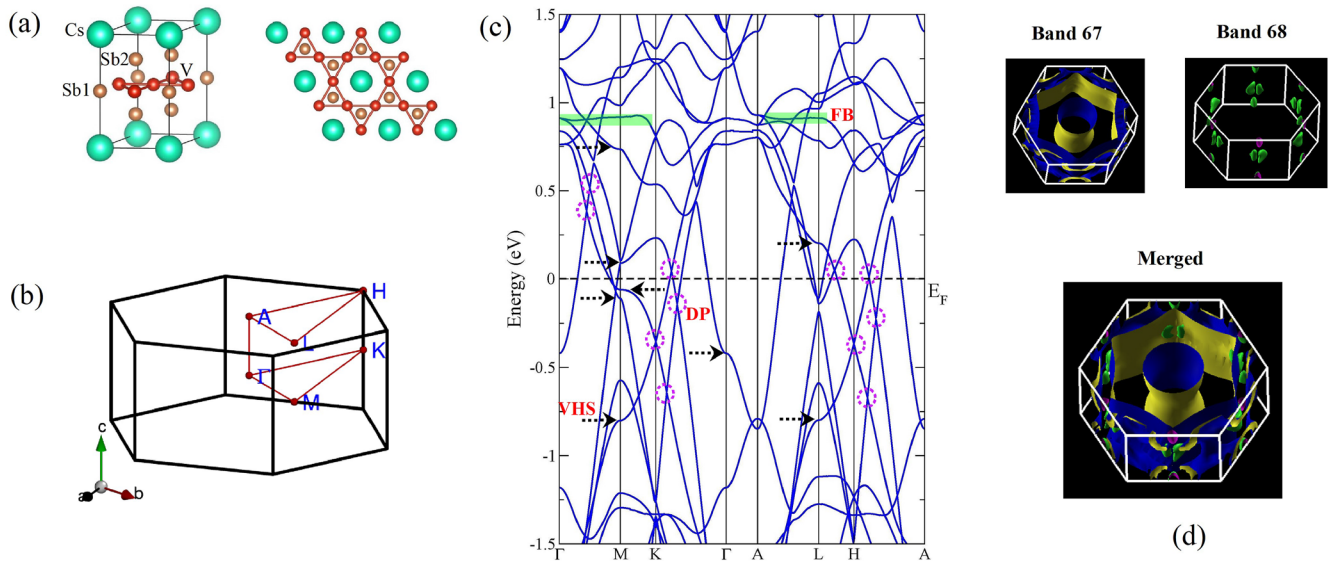

FIG. 1. (a) Unit cell of CsV_3Sb_5 (left panel) and the kagome layer of V atoms (right panel). (b) High-symmetry **k**-path in the first Brillouin zone. (c) Electronic band structure of CsV_3Sb_5 in the pristine phase at ambient pressure. The Dirac points (DPs) near the Fermi level are highlighted with dotted circles, while the van Hove singularities (VHSs) and flat band (FB) are indicated by dashed arrows and the shaded regions, respectively. (d) Band-resolved Fermi surface of CsV_3Sb_5, showing contributions from Band 67 and Band 68. The bottom inset presents the combined Fermi surface from both bands.

The application of uniaxial pressure (along a single direction) is particularly effective in changing the aspect ratio of lattice parameters, thereby shifting specific features of the band structure. This idea emerged due to the feasibility of experimental setups that allow investigations under compressive and tensile stress.[14–17] Several studies have reported the occurrence of superconducting states at high pressure and low temperature. The application of pressure enables controlled deformation of the crystal structure, which ultimately allows fine-tuning of the band structure without introducing impurities. Multiple superconducting domes have been observed in materials such as KFe_2Se_2, $RbFe_2Se_2$,[18] LiFeOHFeSe,[19] $CeCu_2Si_2$,[20] FeS,[21] and Eu–Ca–Fe_2As_2.[22] The presence of such domes suggests unconventional superconductivity.[23] This has sparked significant research interest in determining whether AV_3Sb_5 also exhibits such multiple superconducting domes under pressure.

Recent pressure-related studies on CsV_3Sb_5 have revealed shifts in van Hove singularities, resulting in changes to the Fermi surface topology and the emergence of new quantum phases.[14–17,24,25] A double-dome superconducting phase diagram has been observed in AV_3Sb_5 within a moderate pressure range of 2 GPa through electrical transport and magnetic susceptibility measurements.[16,26–28] The maximum superconducting transition temperature, T_c, of 8 K occurs at 2 GPa, coinciding with the complete suppression of the CDW phase. Zhang *et al.*[24] reported a gradual reduction in the superconducting phase in CsV_3Sb_5 as pressure increased from 0.8 to 7.5 GPa, with the phase disappearing entirely beyond this range. Interestingly, a reemergence of the CDW phase was observed around 16.5 GPa, persisting robustly up to 47.9 GPa, which has been attributed to a pressure-induced Lifshitz transition. Other groups have also explored the pressure-dependent interplay between CDW order and superconductivity in CsV_3Sb_5 at pressures up to 50 GPa.[17,29]

Despite numerous studies on AV_3Sb_5, a comprehensive understanding of how applied pressure influences electronic correlations and Fermi surface topology in CsV_3Sb_5 has not yet been achieved. Addressing these questions is essential for unraveling the mechanisms behind pressure-induced phase transitions and the complex interplay between CDW and superconductivity in kagome metals. In this study, we conducted systematic pressure-dependent electronic structure analyses of CsV_3Sb_5 using experimentally determined crystal structure files up to 20 GPa. Our results reveal significant changes in the electronic bands, including the shifting and formation of Dirac points near the Fermi level, as well as pressure-induced shifts in flat bands and VHSs. To evaluate lattice stability, we calculated the phonon dispersion at various pressures. At ambient pressure, the presence of negative (or imaginary) phonon frequencies indicates lattice instability, which gradually transitions to positive frequencies above 4.9 GPa. This strongly suggests the dynamical stability of CsV_3Sb_5 under high-pressure conditions.

II. COMPUTATIONAL DETAILS AND NUMERICAL SOFTWARE

Full-potential DFT codes, such as WIEN2k[30] and FPLO (full-potential local-orbital),[31,32] were used for electronic structure calculations and Fermi surface calculations. All codes are based on the full-potential linearized augmented plane wave (FLAPW) method within a DFT framework. All electrons were treated using the standard generalized gradient approximation (GGA) with the parameterization of the Perdew–Burke–Ernzerhof (PBE).[33] The outermost

electron configurations used in the calculations are $5s^2 5p^6 6s^1$ for Cs, $3s^2 3p^6 3d^3 4s^2$ for V, and $4d^{10} 5s^2 5p^3$ for Sb. The Fermi surfaces were generated using 5000 **k**-points, resulting in a dense **k**-point mesh of $28 \times 28 \times 26$. From our DFT calculations, CsV_3Sb_5 was found to be stable with the lowest energy in the nonmagnetic state and exhibits metallic behavior, consistent with experimental reports.[5,34]

The phonon dispersion was computed by solving the equation

$$\sum_{\beta\tau'} D^{\alpha\beta}_{\tau\tau'}(\mathbf{q}) \gamma^{\beta\tau'}_{\mathbf{q}j} = \omega^2_{\mathbf{q}j} \gamma^{\alpha\tau}_{\mathbf{q}j}, \quad (1)$$

where the indices τ, τ' represent the atoms, α, β are the Cartesian coordinates, $\mathbf{q}$ is a wave vector, j is a band index, $D(\mathbf{q})$ represents the dynamical matrix, ω signifies the corresponding phonon frequency, and γ is the polarization vector.

For phonon calculations, the Vienna *ab initio* Simulation Package (VASP) with a set of plane wave basis was employed. The exchange correlation interactions among the electrons were modeled using the PBE functional within the generalized gradient approximation (GGA). The atomic positions of all the atoms present in the structures at different pressure points were fully relaxed using the conjugate gradient algorithm until the energy converged to less than 10^{-8} eV and the forces on each atom were less than 10^{-7} eV/Å. The plane wave basis set was defined using an energy cutoff of 500 eV, and the Brillouin zone was sampled with an $11 \times 11 \times 11$ Monkhorst–Pack **k**-point mesh for structural optimization. Phonon dispersions were calculated using the finite displacement method[35] on a supercell of $3 \times 3 \times 2$ (162 atoms), as implemented in the Phonopy package.[36]

III. RESULTS AND DISCUSSION

To understand the electronic structure of CsV_3Sb_5, we calculated its density of states (DOS) and electronic band structure at ambient pressure (0 GPa) along the high-symmetry **k**-path depicted in Fig. 1(b). The electronic band structure at ambient pressure, shown in Fig. 1(c), reveals several intriguing features, including multiple Dirac-like crossings along the Γ–M–K and L–H–A directions. Most of these Dirac points lie near the Fermi level, as indicated by the dotted circles. Furthermore, the electronic bands possess multiple VHS points and flat bands, as indicated by the dashed arrows and shaded areas, respectively. It is worth noting that there are four VHSs at the M-point, most of which lie very close to the Fermi level. These features of the electronic band structure are consistent with previous DFT reports.[7,37]

To gain a deeper understanding of electronic structure, we calculated the partial and total DOS along with the orbital-resolved band structure of CsV_3Sb_5, as presented in the supplementary material. As shown in Fig. S1, the major contribution to the total DOS around E_F primarily originates from the V-3*d* and Sb-5*p* orbitals. The Fermi level lies within the vanadium *d* orbital. The DOS exhibits a local minimum near E_F, indicating a semi-metallic nature. The orbital-resolved band structure of CsV_3Sb_5 with spin–orbit coupling (SOC) at ambient pressure is illustrated in Fig. S2 in supplementary material. There are two bands (red and blue) crossing E_F around the Γ and A points, and these bands predominantly arise from the out-of-plane Sb-*pz* orbitals, while the bands near the M and L points are dominated by the out-of-plane V-d_{xz}/d_{yz} orbitals.

Furthermore, the Dirac points near E_F, highlighted by dotted circles, are predominantly influenced by the in-plane V-$d_{xy}/d_{x^2-y^2}$ orbitals. It is important to note that a gap opens at some Dirac crossings due to the SOC effect. Multiple VHSs, or saddle points, are identified at the Γ, M, and L points, as marked by dotted arrows (Fig. S2). The VHSs at the L point are primarily contributed by Sb p_z orbitals, whereas those at the *A* and Γ points mainly originate from V-d_{z^2} orbitals. These observations in DOS and electronic bands are in good agreement with previous DFT studies[5,6,14,38] in CsV_3Sb_5. VHSs, due to their large density of states, significantly reduce local Coulomb interactions and play a pivotal role in various Fermi surface instabilities, as corroborated by ARPES experiments.[39]

We also computed the Fermi surface of CsV_3Sb_5. As shown in the electronic band plot [Fig. 1(c)], two bands, Band 67 and Band 68, cross the Fermi level and contribute to the Fermi surface of this material. Figure 1(d) presents the band-resolved Fermi surface of CsV_3Sb_5. The Fermi pocket of Band 67 exhibits a deformed cylindrical shape centered at the Γ point, along with a hexagon-like pocket at the boundary of the Brillouin zone. In contrast, the Fermi pockets of Band 68 take on multiple kidney-like small pockets, which are also located at the boundary of the Brillouin zone. The nearly two-dimensional nature of the Fermi surface in CsV_3Sb_5 indicates strong in-plane bonding and weak inter-layer coupling in this material. The Fermi surface of CsV_3Sb_5 is similar to other kagome materials, such as KV_3Sb_5,[40] (Cs, Rb)Ti_3Bi_5,[41] FeGe,[42] and ScV_6Sn_6.[43]

The electronic structure of CsV_3Sb_5 at ambient pressure is quite intriguing, showcasing multiple notable features, including Dirac points, flat bands, and VHS points. In addition, the Fermi surface exhibits quasi-2D and hexagonal-like pockets at the Γ point and along the boundary of the Brillouin zone. To investigate how these characteristics evolve under pressure, we have conducted a study of the pressure-dependent electronic bands and Fermi surface of this material. Figure 2 shows the electronic bands of CsV_3Sb_5 under pressures of 4.9, 9.8, 15.3, and 20 GPa.

The graph demonstrates that pressure serves as an effective tool for tuning the electronic structure of CsV_3Sb_5. A notable feature that undergoes significant changes with pressure is the emergence of two Dirac points along the Γ–A–L path, as highlighted by the dashed circle. At ambient pressure, there is a simple crossing of two bands at the *A*-point of the Brillouin zone [Fig. 1(c)]. However, at a pressure of 4.9 GPa, this transforms into two Dirac-like crossings [Fig. 2(a)], and intriguingly, these Dirac points move progressively closer to the Fermi level as pressure increases. By 20 GPa, these Dirac points are situated approximately ~25 meV below the Fermi level. The proximity of these pressure-induced Dirac crossings to the Fermi level enhances high mobility and reduces the effective mass of charge carriers, leading to potentially significant improvements in conductivity, thermoelectric performance, and magnetotransport behavior.

Furthermore, the VHS at the Γ point gradually shifts upward as the pressure increases from 0 to 4.9 GPa, crossing the Fermi level at 9.8 GPa, as indicated by the dashed arrow. With further pressure increases to 15.3 and 20 GPa, the VHS continues to rise. The Dirac points also shift under pressure, with the most intriguing

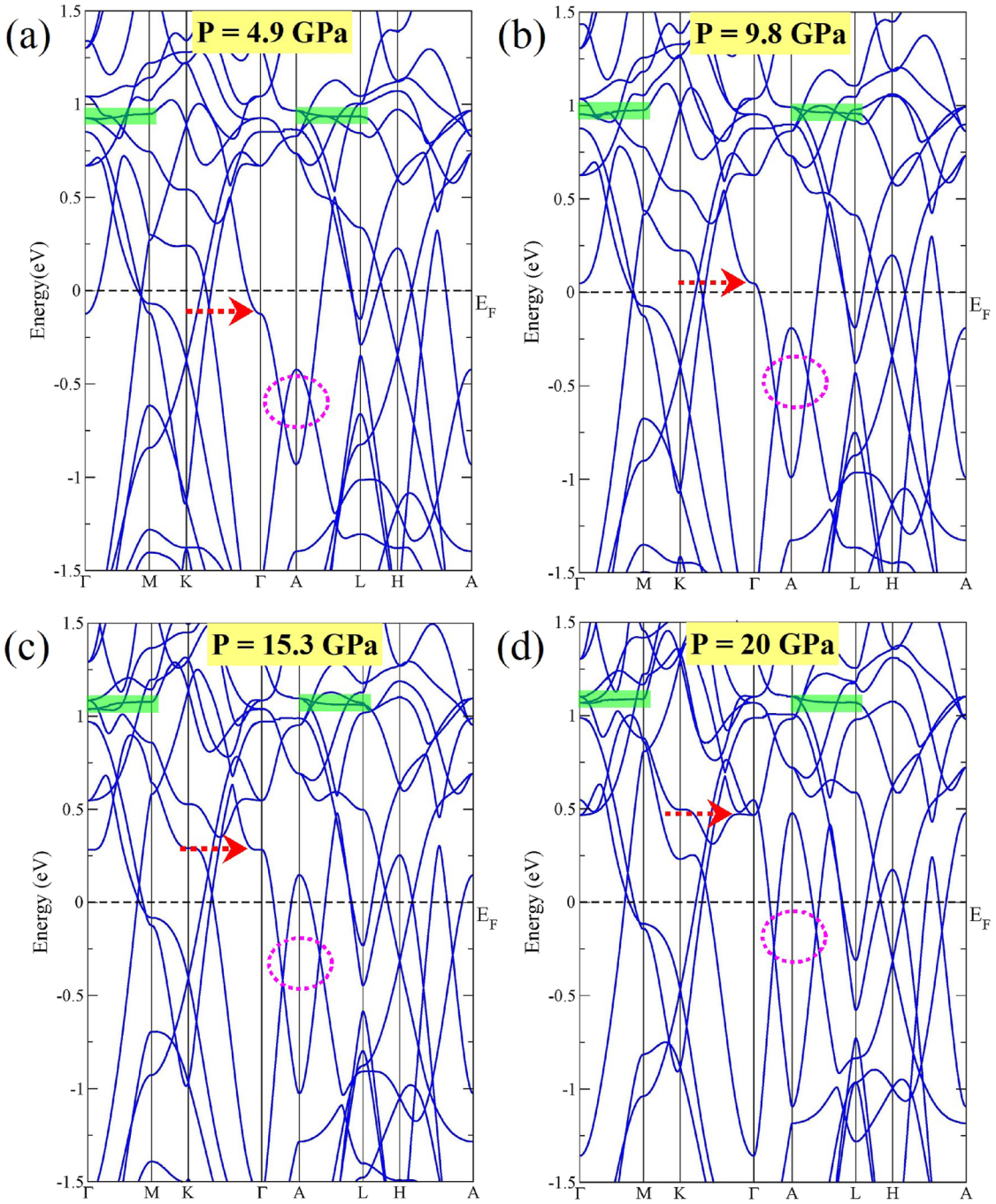

FIG. 2. Electronic band structure of CsV_3Sb_5 along high-symmetry directions at (a) 4.9, (b) 9.8, (c) 15.3, and (d) 20 GPa. The Dirac points and van Hove singularity (VHS) points exhibit noticeable shifts under pressure, while the flat bands appear to remain nearly intact. Notably, the VHS point at the Γ-point crosses the Fermi level as pressure increases from 4.9 to 9.8 GPa. In addition, two new Dirac points emerge at higher pressures and gradually approach the Fermi level.

change being the development of two Dirac points from the band crossings along the Γ–A–L path. These points move closer to the Fermi level, as highlighted by the dotted circles in Fig. 2. Meanwhile, other Dirac points remain nearly unaffected, even at 20 GPa. In addition, the flat bands exhibit a slight upward shift under pressure, as indicated by the shaded area. These observations clearly demonstrate that the electronic structure of CsV_3Sb_5 is highly responsive to external pressure.

As shown in Fig. 3, two bands, Band 67 and Band 68, cross the Fermi level and contribute to the Fermi surface of CsV_3Sb_5. The Fermi pocket of Band 67 exhibits a deformed cylindrical shape centered at the Γ point, along with hexagon-like features at the boundary of the Brillouin zone. In contrast, the Fermi pockets of Band 68 take on multiple kidney-like shapes. With increasing pressure, the Fermi pockets of both bands undergo noticeable deformations. For Band 67, the cylindrical shape shrinks at the center and transforms into two semi-spherical shapes when the pressure exceeds 9.8 GPa. Similarly, other Fermi pockets also display significant deformation as the pressure increases. Our previous high-pressure study in the CDW phase also showed that the Fermi pockets of CsV_3Sb_5 exhibit noticeable changes within a moderate pressure range of 1.49 GPa.[44]

According to Onsager's relation,[45–47] the frequency of de Haas–van Alphen (dHvA) oscillations (f) is directly proportional to the cross-sectional area (A) of the Fermi pocket, given by $f = \frac{\phi_0}{2\pi^2}A$, where $\phi_0 = 2.07 \times 10^{-15}$ T m^2 is the quantum of flux. Therefore, the dHvA oscillation frequency observed in quantum oscillation experiments provides a direct measure of the Fermi surface cross section. In fact, quantum oscillation experiments are a direct probe of the Fermi surface in quantum materials. As shown in Fig. 3, the cross-sectional areas of the Fermi pockets change with pressure, leading to expected variations in the dHvA frequencies at different pressures. Accordingly, we calculated all possible theoretical dHvA oscillation frequencies at various pressure points using Onsager's relation, as illustrated in Fig. 4. For these calculations, we utilized the SKEAF code.[48]

Figure 4 shows the angular dependence of all possible theoretical frequencies for CsV_3Sb_5 under different applied pressures. The frequencies derived from Band 67 are large, reaching up to 9000 T, and vary nearly parabolically at higher tilt angles (θ). This behavior is consistent with expectations for a quasi-2D Fermi surface. Here, θ represents the polar magnetic field angle. In contrast, the frequencies derived from the Fermi pocket of Band 68 are smaller due to their smaller cross-sectional areas and exhibit an increasing trend with rising θ.

To investigate the stability of CsV_3Sb_5 under high-pressure conditions, we calculated the phonon dispersion and phonon DOS at various pressure points: 0, 4.9, 9.8, 15.3, 17.4, and 20 GPa, as illustrated in Fig. 5. These calculations offer valuable insights into the lattice dynamics and stability of the material under structural distortions. At ambient pressure (0 GPa), the phonon dispersion curves exhibit imaginary frequencies (negative values) at the M- and L-points of the Brillouin zone, indicating dynamical instability in the lattice. These imaginary modes suggest the potential for structural distortions or phase transformations at zero pressure.[37,49] As the pressure increases to 4.9 GPa, the imaginary frequencies at the M- and L-points decrease in magnitude, suggesting a gradual stabilization of the lattice under compression.

To investigate how the negative frequency modes gradually transition to positive, we performed phonon calculations at intermediate pressure points (2 and 3 GPa), as shown in Figs. S3 and S4 in the supplementary material. The negative (or imaginary) frequency at the M-point at ambient pressure becomes positive at 2 GPa; however, the frequency at the L-point remains negative, though its magnitude is smaller than at ambient pressure. At 3 GPa, the frequency at the L-point remains negative, with a further reduction in magnitude compared to ambient pressure and 2 GPa.

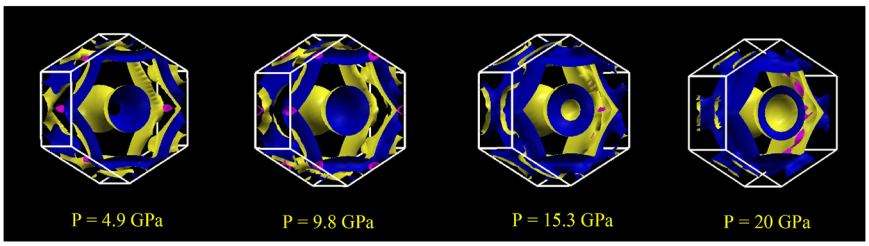

FIG. 3. Fermi surface of CsV_3Sb_5 at pressures of 4.9, 9.8, 15.3, and 20 GPa. The Fermi pockets undergo gradual deformation with increasing pressure. The nearly cylindrical Fermi pocket centered at the Γ-point progressively shrinks at its center, eventually breaking into two upper and lower hemispheres.

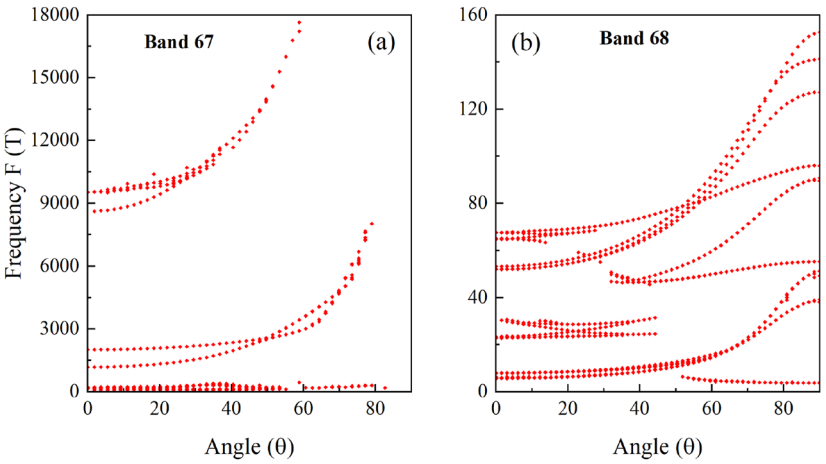

FIG. 4. Angular dependence of de Haas–van Alphen (dHvA) oscillation frequencies of CsV_3Sb_5, computed from the Fermi pockets of (a) Band 67 and (b) Band 68 at ambient pressure. Most frequencies increase gradually with the tilt angle θ, as expected for cylindrical-like Fermi pockets.

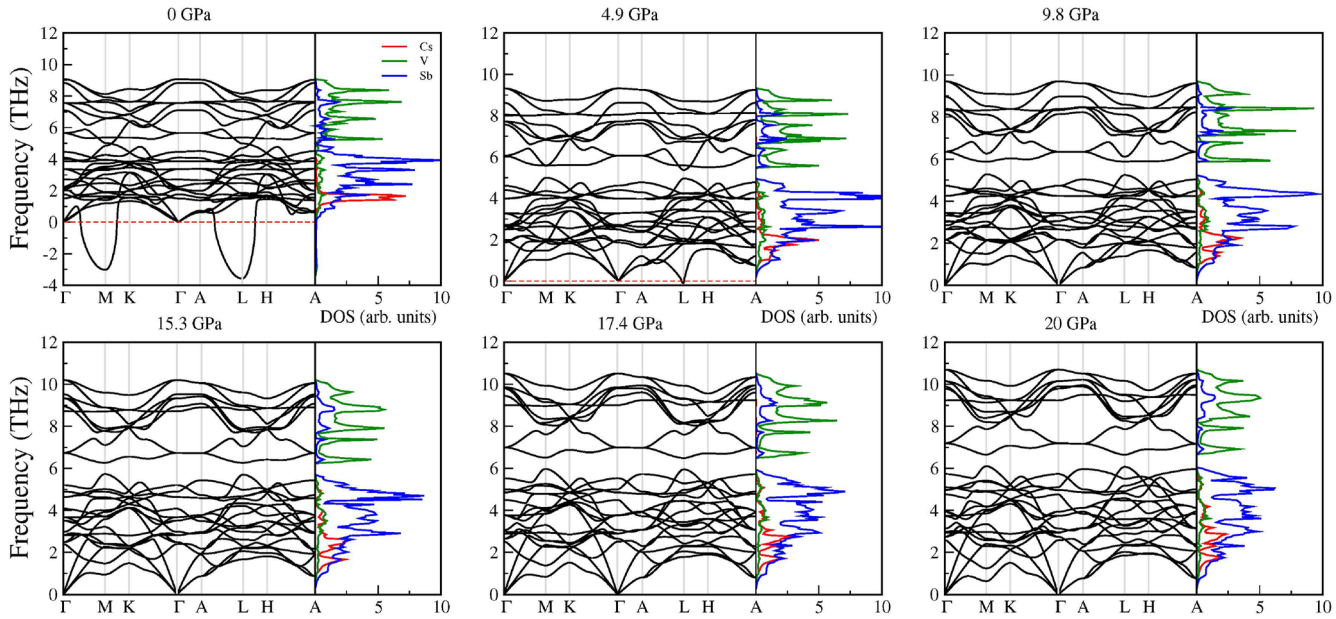

FIG. 5. Phonon dispersion and phonon density of states of CsV_3Sb_5 at pressures of 0, 4.9, 9.8, 15.3, 17.4, and 20 GPa. The imaginary (negative) phonon frequencies along the Γ–M–K and A–L–H directions at 0 GPa indicate lattice instability. At pressures above 4.9 GPa, the phonon frequencies become positive, suggesting lattice stability.

By 9.8 GPa, the phonon spectrum is entirely positive, with no imaginary modes, confirming the dynamical stabilization of the structure. At higher pressures (15.3, 17.4, and 20 GPa), the phonon frequencies across the Brillouin zone shift upward, reflecting bond stiffening and enhanced lattice rigidity. The phonon DOS further supports these findings. At 0 GPa, the DOS includes contributions from imaginary frequencies, consistent with the observed lattice instabilities. With increasing pressure, the DOS evolves, and by 9.8 GPa, the low-frequency states (corresponding to imaginary modes) disappear. At 20 GPa, the DOS features well-defined peaks, with the highest frequency reaching ~12 THz, indicating a fully stabilized lattice.

The presence of imaginary frequencies at ambient and low pressures points to the likelihood of structural distortions or phase transitions under these conditions. In contrast, the stabilization of the phonon spectrum above 9.8 GPa suggests a pressure-induced phase transition to a dynamically stable configuration. In addition, the pressure-induced shifts in phonon frequencies, indicative of increasing lattice rigidity, may have significant implications for the materials' thermal transport properties. These results are significant for understanding the structural and vibrational properties of CsV_3Sb_5 and its potential applications in high-pressure environments.

IV. SUMMARY

In this study, we investigated the evolution of the electronic and structural properties of the kagome metal CsV_3Sb_5 under varying pressure conditions using first-principles density functional theory (DFT). At ambient pressure, the electronic band structure of CsV_3Sb_5 exhibits distinctive features such as Dirac points, van Hove singularity (VHS), and flat bands near the Fermi surface. The VHS demonstrates high sensitivity to external pressure, moving progressively upward toward the Fermi level and crossing it at pressures above 9.8 GPa. Intriguingly, pressure induces Dirac-like crossings in the electronic bands, which approach the Fermi level and stabilize at ~25 meV below it under 20 GPa. The Fermi surface primarily consists of two features: a deformed cylindrical pocket at the Γ point and hexagon-like pockets at the Brillouin zone boundary. With increasing pressure, these features undergo significant deformation, with the cylindrical pocket shrinking and transforming into two semi-spherical pockets at pressures above 4.9 GPa.

The dynamic stability of the high-pressure phases was assessed through phonon dispersion calculations. Consistent with previous DFT studies,[37] CsV_3Sb_5 exhibits structural instability in its pristine phase, as evidenced by softened breathing phonon modes. This instability is linked to the CDW transition, driven by Fermi surface nesting and the VHS. Our phonon calculations under high-pressure conditions reveal that these negative frequency modes gradually transition to positive values above 4.9 GPa, stabilizing consistently up to the maximum investigated pressure of 20 GPa. This behavior indicates that the lattice structure of CsV_3Sb_5 becomes dynamically stable under higher pressures.

These results provide crucial insights into the structural and vibrational properties of CsV_3Sb_5, highlighting its potential for applications in high-pressure environments. Furthermore, they offer valuable contributions to the broader understanding of kagome-based quantum materials and their emergent phenomena.

SUPPLEMENTARY MATERIAL

The supplementary material provides details on the density of states (DOS), electronic band, phonon, and Fermi surface analyses of CsV_3Sb_5 at different pressure points.

ACKNOWLEDGMENTS

The work at West Texas A&M University (WTAMU) was supported by the Welch Foundation (Grant No. AE-0025) and the National Science Foundation (Award ID. 2336011). The computations were performed on the WTAMU HPC cluster, funded by the National Science Foundation (NSF CC GROWTH Grant No. 2018841). D.P.R. and S.R.B. gratefully acknowledge DST, India, for the ISRF research fellowship (Award No. INSA/DST-ISRF/2022/35). We sincerely acknowledge Alexander A. Tsirlin and his team for providing the crystallographic information files used in this research.

AUTHOR DECLARATIONS

Conflict of Interest

The authors have no conflicts to disclose.

Author Contributions

Shalika R. Bhandari: Conceptualization (equal); Data curation (equal); Writing – original draft (equal). **Vivek Gusain**: Conceptualization (equal); Data curation (equal); Writing – original draft (equal). **Mohd Zeeshan**: Conceptualization (equal); Data curation (equal); Writing – original draft (equal). **D. P. Rai**: Conceptualization (equal); Data curation (equal); Writing – original draft (equal). **Keshav Shrestha**: Conceptualization (lead); Data curation (lead); Formal analysis (lead); Investigation (lead); Writing – original draft (lead).

DATA AVAILABILITY

The data that support the findings of this study are available within the article and its supplementary material.

REFERENCES

[1]J.-X. Yin, B. Lian, and M. Z. Hasan, "Topological kagome magnets and superconductors," Nature **612**, 647 (2022).
[2]S. D. Wilson and B. R. Ortiz, "AV_3Sb_5 kagome superconductors," Nat. Rev. Mater. **9**, 420 (2024).
[3]K. Jiang, T. Wu, J.-X. Yin, Z. Wang, M. Z. Hasan, S. D. Wilson, X. Chen, and J. Hu, "Kagome superconductors AV_3Sb_5 (A = K, Rb, Cs)," Natl. Sci. Rev. **10**, nwac199 (2023).
[4]K. Shrestha, M. Shi, T. Nguyen, D. Miertschin, K. Fan, L. Deng, D. E. Graf, X. Chen, and C.-W. Chu, "Fermi surface mapping of the kagome superconductor Rbv_3Sb_5 using de Haas–van alphen oscillations," Phys. Rev. B **107**, 075120 (2023).
[5]B. R. Ortiz, L. C. Gomes, J. R. Morey, M. Winiarski, M. Bordelon, J. S. Mangum, I. W. H. Oswald, J. A. Rodriguez-Rivera, J. R. Neilson, S. D. Wilson *et al.*, "New kagome prototype materials: Discovery of KV_3Sb_5, RbV_3Sb_5, and CsV_3Sb_5," Phys. Rev. Mater. **3**, 094407 (2019).
[6]B. R. Ortiz, S. M. L. Teicher, Y. Hu, J. L. Zuo, P. M. Sarte, E. C. Schueller, A. M. M. Abeykoon, M. J. Krogstad, S. Rosenkranz, R. Osborn *et al.*, "CsV_3Sb_5: A Z_2 topological kagome metal with a superconducting ground state," Phys. Rev. Lett. **125**, 247002 (2020).
[7]M. Kang, S. Fang, J.-K. Kim, B. R. Ortiz, S. H. Ryu, J. Kim, J. Yoo, G. Sangiovanni, D. Di Sante, B.-G. Park *et al.*, "Twofold van Hove singularity and origin of charge order in topological kagome superconductor CsV_3Sb_5," Nat. Phys. **18**, 301 (2022).
[8]K. Shrestha, R. Chapai, B. K. Pokharel, D. Miertschin, T. Nguyen, X. Zhou, D. Y. Chung, M. G. Kanatzidis, J. F. Mitchell, U. Welp *et al.*, "Nontrivial Fermi surface topology of the kagome superconductor CsV_3Sb_5 probed by de Haas–van Alphen oscillations," Phys. Rev. B **105**, 024508 (2022).
[9]J. Zhao, W. Wu, Y. Wang, and S. A. Yang, "Electronic correlations in the normal state of the kagome superconductor KV_3Sb_5," Phys. Rev. B **103**, L241117 (2021).
[10]M. I. Naher, M. A. Ali, M. M. Hossain, M. M. Uddin, and S. H. Naqib, "A comprehensive *ab-initio* insights into the pressure dependent mechanical, phonon, bonding, electronic, optical, and thermal properties of CsV_3Sb_5 kagome compound," Results Phys. **51**, 106742 (2023).
[11]Y. Xie, Y. Li, P. Bourges, A. Ivanov, Z. Ye, J.-X. Yin, M. Z. Hasan, A. Luo, Y. Yao, Z. Wang *et al.*, "Electron-phonon coupling in the charge density wave state of CsV_3Sb_5," Phys. Rev. B **105**, L140501 (2022).
[12]P. Mondal, M. R. Islam, M. S. Khanom, and F. Ahmed, "The impact of hydrostatic pressure on the structural, mechanical, thermal, and optoelectronic characteristics of the RsV_3Sb_5 kagome compound: *Ab initio* approach," ChemistryOpen **14**, e202400291 (2024).
[13]S. R. Bhandari, M. Zeeshan, V. Gusain, K. Shrestha, and D. P. Rai, "First-principles study of the electronic structure, Z_2 invariant, and quantum oscillation in the kagome material CsV_3Sb_5," APL Quantum **1**, 046118 (2024).
[14]H. LaBollita and A. S. Botana, "Tuning the van Hove singularities in AV_3Sb_5 (A= K, Rb, Cs) via pressure and doping," Phys. Rev. B **104**, 205129 (2021).
[15]L. Nie, K. Sun, W. Ma, D. Song, L. Zheng, Z. Liang, P. Wu, F. Yu, J. Li, M. Shan *et al.*, "Charge-density-wave-driven electronic nematicity in a kagome superconductor," Nature **604**, 59 (2022).
[16]K. Y. Chen, N. N. Wang, Q. W. Yin, Y. H. Gu, K. Jiang, Z. J. Tu, C. S. Gong, Y. Uwatoko, J. P. Sun, H. C. Lei *et al.*, "Double superconducting dome and triple enhancement of T_c in the kagome superconductor CsV_3Sb_5 under high pressure," Phys. Rev. Lett. **126**, 247001 (2021).
[17]J.-G. Si, W.-J. Lu, Y.-P. Sun, P.-F. Liu, and B.-T. Wang, "Charge density wave and pressure-dependent superconductivity in the kagome metal CsV_3Sb_5: A first-principles study," Phys. Rev. B **105**, 024517 (2022).
[18]L. Sun, X.-J. Chen, J. Guo, P. Gao, Q.-Z. Huang, H. Wang, M. Fang, X. Chen, G. Chen, Q. Wu *et al.*, "Re-emerging superconductivity at 48 kelvin in iron chalcogenides," Nature **483**, 67 (2012).
[19]J. P. Sun, P. Shahi, H. X. Zhou, Y. L. Huang, K. Y. Chen, B. S. Wang, S. L. Ni, N. N. Li, K. Zhang, W. G. Yang *et al.*, "Reemergence of high-T_c superconductivity in the $(Li_{1-x}Fe_x)OHFe_{1-y}Se$ under high pressure," Nat. Commun. **9**, 380 (2018).
[20]H. Q. Yuan, F. M. Grosche, M. Deppe, C. Geibel, G. Sparn, and F. Steglich, "Observation of two distinct superconducting phases in $CeCu_2Si_2$," Science **302**, 2104 (2003).
[21]J. Zhang, F.-L. Liu, T.-P. Ying, N.-N. Li, Y. Xu, L.-P. He, X.-C. Hong, Y.-J. Yu, M.-X. Wang, J. Shen *et al.*, "Observation of two superconducting domes under pressure in tetragonal FeS," npj Quantum Mater. **2**, 49 (2017).
[22]K. Shrestha, L. Z. Deng, K. Zhao, B. I. Jawdat, B. Lv, B. Lorenz, and C. W. Chu, "Doping dependence and high-pressure studies on $Eu_xCa_{1-x}Fe_2As_2$ $(0 \le x \le 1)$," Supercond. Sci. Technol. **33**, 095010 (2020).
[23]T. Das and C. Panagopoulos, "Two types of superconducting domes in unconventional superconductors," New J. Phys. **18**, 103033 (2016).
[24]Z. Zhang, Z. Chen, Y. Zhou, Y. Yuan, S. Wang, J. Wang, H. Yang, C. An, L. Zhang, X. Zhu *et al.*, "Pressure-induced reemergence of superconductivity in the topological kagome metal CsV_3Sb_5," Phys. Rev. B **103**, 224513 (2021).
[25]L. Zheng, Z. Wu, Y. Yang, L. Nie, M. Shan, K. Sun, D. Song, F. Yu, J. Li, D. Zhao *et al.*, "Emergent charge order in pressurized kagome superconductor CsV_3Sb_5," Nature **611**, 682 (2022).
[26]F. Du, S. Luo, B. R. Ortiz, Y. Chen, W. Duan, D. Zhang, X. Lu, S. D. Wilson, Y. Song, and H. Yuan, "Pressure-induced double superconducting domes and charge instability in the kagome metal KV_3Sb_5," Phys. Rev. B **103**, L220504 (2021).

[27]C. C. Zhu, X. F. Yang, W. Xia, Q. W. Yin, L. S. Wang, C. C. Zhao, D. Z. Dai, C. P. Tu, B. Q. Song, Z. C. Tao *et al.*, "Double-dome superconductivity under pressure in the v-based kagome metals AV_3Sb_5 (A= Rb and K)," Phys. Rev. B **105**, 094507 (2022).
[28]N. N. Wang, K. Y. Chen, Q. W. Yin, Y. N. N. Ma, B. Y. Pan, X. Yang, X. Y. Ji, S. L. Wu, P. F. Shan, S. X. Xu *et al.*, "Competition between charge-density-wave and superconductivity in the kagome metal RbV_3Sb_5," Phys. Rev. Res. **3**, 043018 (2021).
[29]X. Chen, X. Zhan, X. Wang, J. Deng, X.-B. Liu, X. Chen, J.-G. Guo, and X. Chen, "Highly robust reentrant superconductivity in CsV_3Sb_5 under pressure," Chin. Phys. Lett. **38**, 057402 (2021).
[30]P. Blaha, K. Schwarz, G. K. Madsen, D. Kvasnicka, and J. Luitz, "WIEN2K, An augmented plane wave+ local orbitals program for calculating crystal properties," edited by K. Schwarz (Vienna University of Technology, Austria, 2001).
[31]K. Koepernik and H. Eschrig, "Full-potential nonorthogonal local-orbital minimum-basis band-structure scheme," Phys. Rev. B **59**, 1743 (1999).
[32]I. Opahle, K. Koepernik, and H. Eschrig, "Full-potential band-structure calculation of iron pyrite," Phys. Rev. B **60**, 14035 (1999).
[33]J. P. Perdew, K. Burke, and M. Ernzerhof, "Generalized gradient approximation made simple," Phys. Rev. Lett. **77**, 3865 (1996).
[34]E. M. Kenney, B. R. Ortiz, C. Wang, S. D. Wilson, and M. J. Graf, "Absence of local moments in the kagome metal KV_3Sb_5 as determined by muon spin spectroscopy," J. Phys.: Condens. Matter **33**, 235801 (2021).
[35]G. Kresse and J. Furthmüller, "Efficient iterative schemes for *ab initio* total-energy calculations using a plane-wave basis set," Phys. Rev. B **54**, 11169 (1996).
[36]A. Togo and I. Tanaka, "First principles phonon calculations in materials science," Scr. Mater. **108**, 1 (2015).
[37]H. Tan, Y. Liu, Z. Wang, and B. Yan, "Charge density waves and electronic properties of superconducting kagome metals," Phys. Rev. Lett. **127**, 046401 (2021).
[38]A. Tsirlin, P. Fertey, B. R. Ortiz, B. Klis, V. Merkl, M. Dressel, S. Wilson, and E. Uykur, "Role of Sb in the superconducting kagome metal CsV_3Sb_5 revealed by its anisotropic compression," SciPost Phys. **12**, 049 (2022).
[39]Y. Hu, X. Wu, B. R. Ortiz, S. Ju, X. Han, J. Ma, N. C. Plumb, M. Radovic, R. Thomale, S. D. Wilson *et al.*, "Rich nature of van Hove singularities in kagome superconductor CsV_3Sb_5," Nat. Commun. **13**, 2220 (2022).
[40]K. Shrestha, M. Shi, B. Regmi, T. Nguyen, D. Miertschin, K. Fan, L. Z. Deng, N. Aryal, S.-G. Kim, D. E. Graf *et al.*, "High quantum oscillation frequencies and nontrivial topology in kagome superconductor KV_3Sb_5 probed by torque magnetometry up to 45 T," Phys. Rev. B **107**, 155128 (2023).
[41]Z. Rehfuss, C. Broyles, D. Graf, Y. Li, H. Tan, Z. Zhao, J. Liu, Y. Zhang, X. Dong, H. Yang *et al.*, "Quantum oscillations in kagome metals $CsTi_3Bi_5$ and $RbTi_3Bi_5$," Phys. Rev. Mater. **8**, 024003 (2024).
[42]K. Tang, H. Zhou, H. Li, S. Pan, X. Wu, H. Li, N. Zhang, C. Xi, J. Zhang, A. Wang *et al.*, "Evidence for unfolded Fermi surfaces in the charge-density-wave state of kagome metal FeGe revealed by de Haas–van Alphen effect," Phys. Rev. Res. **6**, 013276 (2024).
[43]K. Shrestha, B. Regmi, G. Pokharel, S.-G. Kim, S. D. Wilson, D. E. Graf, B. A. Magar, C. Phillips, and T. Nguyen, "Electronic properties of kagome metal ScV_6Sn_6 using high-field torque magnetometry," Phys. Rev. B **108**, 245119 (2023).
[44]C. Phillips, K. Shtefiienko, T. Nguyen, A. N. Capa Salinas, B. A. Magar, G. Pokharel, S. D. Wilson, D. E. Graf, and K. Shrestha, "Fermi surface reconstruction under pressure in the kagome metal CsV_3Sb_5," Phys. Rev. B **110**, 205135 (2024).
[45]D. Shoenberg, *Magnetic Oscillations in Metals* (Cambridge University Press, 2009).
[46]Y. Ando, "Topological insulator materials," J. Phys. Soc. Jpn. **82**, 102001 (2013).
[47]T. Nguyen, N. Aryal, B. K. Pokharel, L. Harnagea, D. Mierstchin, D. Popović, D. E. Graf, and K. Shrestha, "Fermiology of the dirac type-II semimetal candidates (Ni, Zr)Te_2 using de Haas–van Alphen oscillations," Phys. Rev. B **106**, 075154 (2022).
[48]P. M. C. Rourke and S. R. Julian, "Numerical extraction of de Haas–van Alphen frequencies from calculated band energies," Comput. Phys. Commun. **183**, 324 (2012).
[49]H. Tan and B. Yan, "Abundant lattice instability in kagome metal ScV_6Sn_6," Phys. Rev. Lett. **130**, 266402 (2023).